



**HAL**  
open science

# Mechanism of formation of engineered magnesite: A useful mineral to mitigate CO<sub>2</sub> industrial emissions

German Montes-Hernandez, Mamadou Bah, François Renard

## ► To cite this version:

German Montes-Hernandez, Mamadou Bah, François Renard. Mechanism of formation of engineered magnesite: A useful mineral to mitigate CO<sub>2</sub> industrial emissions. *Journal of CO<sub>2</sub> Utilization*, 2020, 35, pp.272-276. 10.1016/j.jcou.2019.10.006 . hal-02896886

**HAL Id: hal-02896886**

**<https://hal.science/hal-02896886>**

Submitted on 5 Nov 2020

**HAL** is a multi-disciplinary open access archive for the deposit and dissemination of scientific research documents, whether they are published or not. The documents may come from teaching and research institutions in France or abroad, or from public or private research centers.

L'archive ouverte pluridisciplinaire **HAL**, est destinée au dépôt et à la diffusion de documents scientifiques de niveau recherche, publiés ou non, émanant des établissements d'enseignement et de recherche français ou étrangers, des laboratoires publics ou privés.

1           **Mechanism of the formation of engineered magnesite: A useful**  
2                           **mineral to mitigate CO<sub>2</sub> industrial emissions**

3  
4                           German Montes-Hernandez<sup>a\*</sup>, Mamadou Bah<sup>a</sup>, François Renard<sup>a,b</sup>

5  
6           <sup>a</sup> Univ. Grenoble Alpes, Univ. Savoie Mont Blanc, CNRS, IRD, IFSTTAR, ISTERre, 38000  
7           Grenoble, France

8           <sup>b</sup> The Njord Centre, PGP, Department of Geosciences, University of Oslo, box 1048 Blindern, 0316  
9           Oslo, Norway

10  
11  
12  
13           \*Corresponding author: G. Montes-Hernandez

14           E-mail address: [german.montes-hernandez@univ-grenoble-alpes.fr](mailto:german.montes-hernandez@univ-grenoble-alpes.fr)

18

## Abstract

19 Magnesium carbonate production at the industrial scale is a realistic option to reduce the industrial  
20 emissions of CO<sub>2</sub>. Ultrabasic rocks and/or alkaline mine waste provide magnesium sources and are  
21 widely available in the Earth's crust. Here, we investigated the aqueous carbonation of magnesium  
22 hydroxide under moderate temperature (25-90°C) and pressure (initial pressure of CO<sub>2</sub>=50 bar)  
23 using NaOH as the CO<sub>2</sub> sequestering agent. From time-resolved Raman measurements, we  
24 demonstrate that the aqueous carbonation of magnesium hydroxide can be an effective engineered  
25 method to trap CO<sub>2</sub> into a solid material and produce large amounts of magnesite MgCO<sub>3</sub> (6  
26 kg/m<sup>3</sup>h), or hydromagnesite Mg<sub>5</sub>(CO<sub>3</sub>)<sub>4</sub>(OH)<sub>2</sub>·4H<sub>2</sub>O (120 kg/m<sup>3</sup>h) at 90°C or nesquehonite  
27 MgCO<sub>3</sub>·3H<sub>2</sub>O (40 kg/m<sup>3</sup>h) at 25°C. Higher production rates were measured for nesquehonite (at  
28 25°C) and hydromagnesite (at 60 and 90°C). However, only the magnesite produced at 90°C  
29 ensures a permanent CO<sub>2</sub> storage because this mineral is the most stable Mg carbonate under Earth  
30 surface conditions, and it could be co-used as construction material in roadbeds, bricks with fire-  
31 retarding property and granular fill. The use of specific organic additives can reduce the reaction  
32 temperature to precipitate magnesite. For example, ferric EDTA (ethylenediaminetetraacetic acid)  
33 reduces the temperature from 90 to 60°C. However, more time is required to complete magnesite  
34 precipitation reaction at this lower temperature (15h at 90°C and 7 days at 60°C). These results  
35 suggests that functionalized organic groups can reduce the energetic barriers during mineral  
36 nucleation.

37

38

39 **Keywords:** Engineered Magnesite Precipitation; Time-Resolved Raman Spectroscopy; Carbon  
40 Dioxide Mineralization; CO<sub>2</sub> Mitigation; Mineral Nucleation and Growth

41

42

43

44

45

46

47

48

49

50

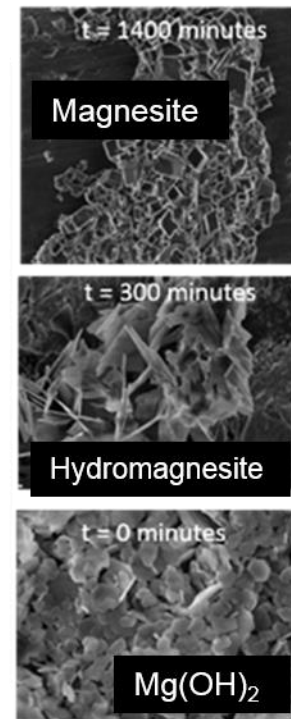
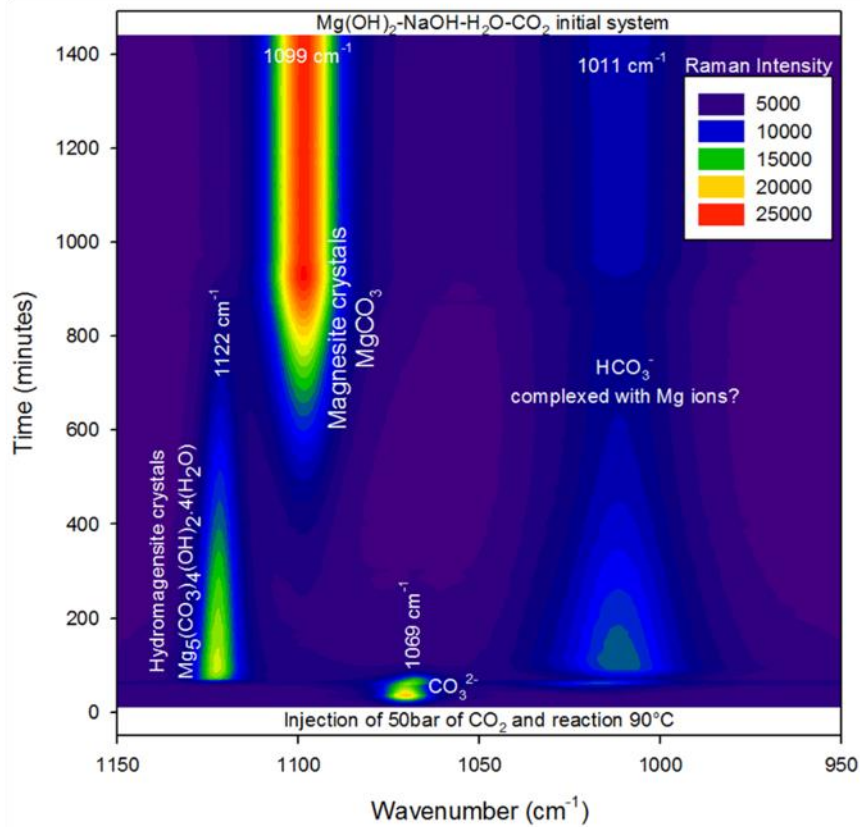
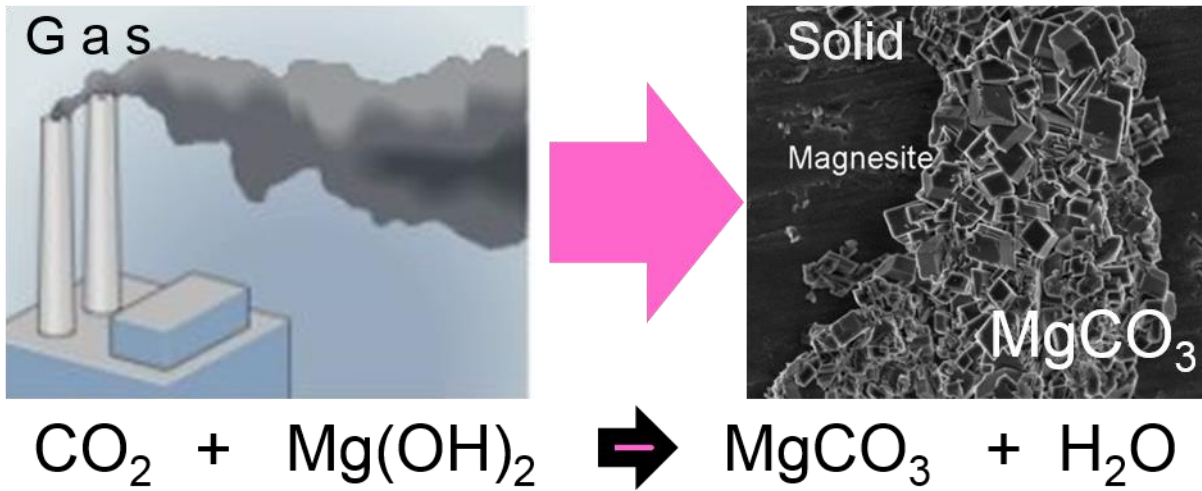
51

52

53

54

55



## 60 **1. Introduction**

61 CO<sub>2</sub> emissions have increased since the industrial revolution: about 36 Gt of CO<sub>2</sub> that  
62 originate from fossil fuel are annually emitted into the atmosphere with 30% from industrial  
63 activities and 70% from transport, agriculture and other sources [1]. These non-regulated emissions  
64 have led to concerns about global warming as a progressive increase of CO<sub>2</sub> concentration into  
65 atmosphere has been recorded in the last two centuries [1]. The energy transition (i.e., the use of  
66 carbon-free energy sources such as hydrogen, solar, wind, marine, hydraulic, geothermal) could  
67 significantly decrease CO<sub>2</sub> emissions. Some limitations, such as the supply of rare Earth elements,  
68 large amounts of water requirements and natural risks, have raised some concerns about how fast  
69 this transition will occur [2-3]. Moreover, conventional and unconventional fossil resources (gas,  
70 carbon and oil) are still available in geological formations [4], and their exploitation and resulting  
71 CO<sub>2</sub> emissions have been predicted to continue for 50-100 years [5]. Therefore, CO<sub>2</sub> capture from  
72 industrial sources and its transformation into re-usable products (e.g. ethanol, syngas, etc.) and/or  
73 non-energetic materials (e.g. calcite, magnesite, siderite, etc.) has been proposed to reduce CO<sub>2</sub>  
74 emissions into the atmosphere [6-9]. CO<sub>2</sub> capture from industrial sources does not represent a  
75 technological or scientific obstacle, but the existing methods and technologies (including recovery  
76 of high-purity of CO<sub>2</sub> and its liquefaction) remain highly expensive. In this way, the improvement  
77 and optimization on the CO<sub>2</sub> capture units still represent important challenges. The goal of the  
78 present experimental study is to demonstrate that engineered magnesite (MgCO<sub>3</sub>) could be used as  
79 an effective option to store carbon dioxide within magnesite-rich solids. The obtained magnesite-  
80 rich solids could then be used as civil construction materials (e.g. roadbed materials, bricks,  
81 granular fill) [10]. Magnesite is the most stable carbonate mineral under typical Earth surface

82 conditions, with the highest resistance to leaching and weathering [11]. The magnesite dissolution  
83 rate is 100-1000 times lower than that of calcite in a wide range of conditions, from ambient  
84 temperature to 150°C and pH from 1 to 14 [11]. For this reason, anhydrous magnesium carbonates  
85 (magnesite and dolomite) have been considered as relevant minerals to store permanently  
86 anthropogenic carbon dioxide. Magnesite and dolomite precipitation kinetics have been widely  
87 studied because their abiotic precipitation at ambient temperature (~25°C) is virtually impossible  
88 within typical experimental time scales [12-13]. The strong solvation shells of magnesium ions in  
89 aqueous media produces this limitation [12]. However, the sole effect of Mg hydration might not  
90 be the only factor of inhibition of magnesite and/or dolomite formation. Recent studies claim that  
91 a more intrinsic crystallization barrier and the influence of fluid chemistry (e.g., relative size of the  
92 constituting cations) prevent the formation of a long-range ordered crystallographic structures at  
93 ambient conditions [14-15]. Conversely, a recent study has reported magnesite precipitation in  
94 batch reactors at room temperature after 77 days of reaction with the aid of carboxylated  
95 polystyrene microspheres [16]. Diluted ionic solutions (<0.1M) and microspheres coated with a  
96 high density of carboxyl groups at their surface allowed the binding and dehydration of Mg<sup>2+</sup> ions  
97 in solution, thereby minimizing the kinetic barrier and facilitating magnesite formation [16].  
98 However, the reaction mechanism and the nature of precipitating minerals between 1 and 77 days  
99 remain to be identified, and whether precipitation occurred via the formation of transient phases or  
100 by a direct nucleation event is unknown. Moreover, this method needs to be up-scaled to produce  
101 high-amounts of magnesite in reasonable time (24 hours). In order to overcome these limitations,  
102 the present study demonstrates magnesite precipitation at moderate temperature (60 and 90°C) by  
103 aqueous carbonation of magnesium hydroxide (Mg(OH)<sub>2</sub>) under anisobaric conditions (initial CO<sub>2</sub>  
104 pressure = 50 bar). These conditions allow the production of high amounts of magnesite in only

105 15h at 90°C or 7 days at 60°C. Herein, NaOH was used as a CO<sub>2</sub> sequestering agent and the ferric  
106 EDTA as a dehydration agent of Mg<sup>2+</sup> ions. Magnesium hydroxide was chosen because its  
107 engineered production from olivine and serpentine-rich materials was actively investigated for CO<sub>2</sub>  
108 mineralization purpose [17-18]. Magnesium oxide (MgO) and magnesium hydroxide (Mg(OH)<sub>2</sub>)  
109 may be produced from serpentine and other Mg-rich silicates. Both synthesized minerals have  
110 numerous industrial applications, and have been proposed as sinks to store anthropogenic carbon  
111 dioxide by transforming it into magnesium carbonate minerals [17-18].

112

## 113 **2. Materials and Methods**

### 114 *2.1. Magnesite precipitation using NaOH as sequestering agent of CO<sub>2</sub>*

115 As already demonstrated in our group (e.g. [8, 19]), the NaOH enhances the magnesite precipitation  
116 at 90°C via aqueous carbonation process of magnesium hydroxide with compressed CO<sub>2</sub>. An initial  
117 CO<sub>2</sub> pressure of 50bar ensures an excess of CO<sub>2</sub> with respect to Mg(OH)<sub>2</sub> in the reactor and ideal  
118 gas condition. In the present study, two new experiments were performed at 90 and 27°C,  
119 respectively, and monitored by time-resolved in situ Raman spectroscopy as described in Montes-  
120 Hernandez and Renard, 2016 [19]. Herein, carbonate speciation and precipitated particles were  
121 monitored for 24h with a 1-minute spectral acquisition time. The Raman spectra were treated in  
122 order to estimate the position, full wide half maximum (FWHM) and integrated surface area as a  
123 function of time for specific stronger peaks in order to explain the reaction mechanism and kinetics  
124 of Mg carbonates precipitation and particularly magnesite (MgCO<sub>3</sub>).

125



126 *2.2. Magnesite precipitation using NaOH and organic additives*

127 Magnesite precipitation was also investigated at 60°C in the presence of three organic molecules  
128 (Aspartame, ferric EDTA, and citric acid tri-sodium salt), expecting a dehydration effect of Mg<sup>2+</sup>  
129 ions or a chelation effect. In these experiments, 15 g of Mg(OH)<sub>2</sub>, provided by Sigma-Aldrich with  
130 chemical purity of 99%, 20g of NaOH, 1 g of organic additive, and 500 mL of high-purity water  
131 were mixed in the reactor (total internal volume of 960 mL). The slurry was immediately dispersed  
132 by mechanical agitation (400 rpm) and gaseous CO<sub>2</sub>, provided by Linde Gas S.A., was injected at  
133 50 bar into the reactor. About 3 minutes at 25°C were required to reach the pre-defined pressure.  
134 The agitation speed was kept to 400 rpm using a rotor with two blades (Parr reactor) that ensured  
135 homogeneous dispersion of reacting and precipitating solids and fast dispersion of the injected CO<sub>2</sub>  
136 in the system. Following injection, the system was heated to 60°C, the pH of the solution and the  
137 CO<sub>2</sub> consumption (pressure drop) were monitored in-situ during mineral formation for 24, 72 or  
138 168 hours.

139 At the end of the experiment, the residual CO<sub>2</sub> was degassed from the reactor by opening the gas  
140 line valve for five minutes. The solid product was recovered by centrifugation and washed twice  
141 with ultrapure water and then was dried directly in the centrifugation flasks at 60 °C for 48 h. The  
142 dry solid products were stored in plastic flasks for subsequent characterization by Raman  
143 spectroscopy, Field Emission Gun Scanning Electron Microscopy (FESEM) and powder X-ray  
144 diffraction (XRD). All ten performed experiments are summarized in Table 1.

145

146

147 *2.3. Ex situ characterization of precipitates*

148 XRD analyses were performed using a Siemens D5000 diffractometer in Bragg-Brentano  
149 geometry, equipped with a theta-theta goniometer with a rotating sample holder. Diffraction  
150 patterns were collected using Cu  $k\alpha_1$  ( $\lambda_{k\alpha_1}=1.5406 \text{ \AA}$ ) and  $k\alpha_2$  ( $\lambda_{k\alpha_2}=1.5444 \text{ \AA}$ ) radiation in the  
151 range  $2\theta = 10 - 70^\circ$ , with a step size of  $0.04^\circ$  and a counting time of 6 seconds per step. For high-  
152 resolution imaging, the solid products were dispersed by ultrasonic treatment in absolute ethanol  
153 for five to ten minutes. One or two droplets of the suspension were then deposited directly on an  
154 aluminum support and coated with platinum. The morphology of the crystals was imaged using a  
155 Zeiss Ultra 55 FESEM with a maximum spatial resolution of approximately 1 nm at 15kV.

156 *2.4. Calculation of production rate*

157 The production rate of a given magnesium carbonate was calculated as follows:

158 
$$P_{\text{rate}} = (\lambda * \text{Mol}_{\text{Mg(OH)}_2} * M_{\text{MgCarbonate}}) / (t_{\text{max}} * V_{\text{reactor}})$$

159 where  $\lambda$  is the chemical conversion factor for Mg carbonate phases determined from Raman  
160 spectroscopy when peaks intensity is constant for a given time-interval. The value  $\lambda=1$  is reached  
161 when the peak intensity for a given Mg carbonate is constant and only a single mineral is detected.  
162  $\text{Mol}_{\text{Mg(OH)}_2}$  is the initial amount (in mol) of  $\text{Mg(OH)}_2$  (complete transformation was determined  
163 from ex-situ XRD measurements in recovered solid products);  $M_{\text{MgCarbonate}}$  is the molar mass of a  
164 given Mg carbonate;  $t_{\text{max}}$  is the time where only one mineral phase exists and the peak intensity is  
165 constant;  $V_{\text{reactor}}$  is the effective volume of the reactor which is equal to 0.6L (runs 1-2) or 1L (runs  
166 3-10). This calculation using time-resolved experimental measurements could allow a realistic  
167 extrapolation to pilot and/or industrial scale assuming roughly proportional dimensions and

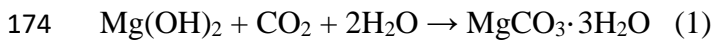
168 equivalent precipitation times.

169

### 170 **3. Results and discussion**

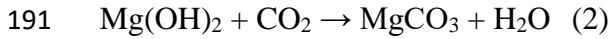
#### 171 *3.1. Magnesite precipitation at 90°C: Reaction mechanism and kinetics*

172 Carbonation of Mg(OH)<sub>2</sub> at 25°C leads the precipitation of nesquehonite, with the following global  
173 reaction:

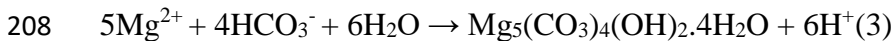


175 The successive events involved during magnesium hydroxide carbonation are displayed in Fig. 1.  
176 Dissolved NaOH enhanced the rate and amount of sequestration of injected CO<sub>2</sub> (initial P<sub>CO2</sub> =50  
177 bar). The carbon dioxide dissolved into interacting alkaline solution (CO<sub>2(gas)</sub> ↔ CO<sub>2(aq)</sub>) was  
178 rapidly dissociated into CO<sub>3</sub><sup>2-</sup> (CO<sub>2(aq)</sub> + 2NaOH → CO<sub>3</sub><sup>2-</sup> + H<sub>2</sub>O + 2Na<sup>+</sup>). A fraction of the  
179 carbonate ions was protonated after about 60 minutes (CO<sub>3</sub><sup>2-</sup> + H<sup>+</sup> → HCO<sub>3</sub><sup>-</sup>) producing a pH change  
180 in the interacting solution, and simultaneously enhancing the dissolution of magnesium hydroxide  
181 (Mg(OH)<sub>2</sub> → Mg<sup>2+</sup> + 2OH<sup>-</sup>). All these combined reactions led to the precipitation of nesquehonite  
182 (Mg<sup>2+</sup> + HCO<sub>3</sub><sup>-</sup> + 3H<sub>2</sub>O → MgCO<sub>3</sub>·3H<sub>2</sub>O + H<sup>+</sup>) with a nucleation induction time of 105 minutes.  
183 This mineral grew by continuous dissolution of magnesium hydroxide until complete consumption  
184 in the reactor. Nesquehonite remained stable in the interacting solution until the end of experiment  
185 (72 h). Ex-situ FESEM images revealed micrometric crystals of prismatic elongated morphology  
186 (Fig. SI-1). Time-resolved Raman measurements and ex-situ characterization of solid confirm that  
187 magnesite precipitation was inhibited by nesquehonite precipitation at 25°C. Conversely,  
188 magnesite formation was rapidly obtained at 90°C and only 15 h were required to produce high-  
189 purity magnesite (~6 kg/m<sup>3</sup>h) as monitored by Raman spectroscopy (Fig. 2). The global reaction

190 summarizes the process:



192 A complete aqueous carbonation reaction was obtained at 90°C exclusively when NaOH was used  
193 as the CO<sub>2</sub> sequestering agent, in agreement with previous results [8]. In the present study, a more  
194 detailed reaction mechanism and kinetics are demonstrated from the time-resolved in-situ Raman  
195 spectroscopy measurements and all temporal reaction events are shown in Fig. 2 and Fig. SI-2.  
196 Similar to the nesquehonite case, the aqueous carbon dioxide ( $\text{CO}_{2(\text{gas})} \leftrightarrow \text{CO}_{2(\text{aq})}$ ) was rapidly  
197 dissociated into  $\text{CO}_3^{2-}$  ( $\text{CO}_{2(\text{aq})} + 2\text{NaOH} \rightarrow \text{CO}_3^{2-} + \text{H}_2\text{O} + 2\text{Na}^+$ ), but this reaction remained active  
198 only during the first 100 minutes. Then, carbonate ions were rapidly protonated, forming  
199 bicarbonate ions ( $\text{CO}_3^{2-} + \text{H}^+ \rightarrow \text{HCO}_3^-$ ) that may complex with  $\text{Mg}^{2+}$ , leading to a shift of the  
200 maximum of the Raman peak of  $\text{HCO}_3^-$  from 1020  $\text{cm}^{-1}$  (Fig.1) to 1011  $\text{cm}^{-1}$  (Fig. 2). After 150  
201 minutes, aqueous carbon dioxide and bicarbonate ions were the dominant species in the reactor,  
202 which induced a significant pH change in the interacting solution as suggested from carbonate  
203 speciation in relation with pH (inorganic carbonate fraction vs pH diagram). Under these  
204 conditions, the dissolution of magnesium hydroxide ( $\text{Mg}(\text{OH})_2 \rightarrow \text{Mg}^{2+} + 2\text{OH}^-$ ) was enhanced,  
205 and the release of magnesium ions generated oversaturation states with respect to several  
206 magnesium carbonates. Consequently, the nucleation of hydromagnesite was detected in-situ after  
207 60 minutes of reaction (first nucleation-event).



209 Hydromagnesite formed as a transient mineral phase that reached a maximum spectral intensity  
210 after 120 minutes. Then, this mineral dissolved in a destabilization processes through a decrease of  
211 spectral peak surface area (i.e., Fig. 3) progressively before the nucleation of magnesite that was  
212 detected after 240 minutes of reaction (second nucleation-event).



214 After this magnesite nucleation event, the growth of magnesite was mainly nourished by  
215 progressive dissolution of hydromagnesite. The temporal evolution of peak surface areas and Full  
216 Width Half Maximum (FWHM) for hydromagnesite and magnesite minerals (Figs. 3 and 4)  
217 suggest that this reaction included coupled dissolution-reprecipitation. Hydromagnesite was  
218 completely consumed after 13 h. An Ostwald ripening process could explain the growth in the  
219 following two hours. Equilibrium was reached after 15 h of reaction, as demonstrated by the  
220 constant FWHM of magnesite after this time (Fig. 4). FESEM images revealed rhombohedral  
221 single crystals with sizes  $<5 \mu\text{m}$  (Fig. SI-3), in agreement with previous work [8].

222

### 223 *3.2. Role of temperature and organic additives*

224 Several complementary experiments were performed in order to assess the evolution of pH in-situ,  
225 the dehydration effect of organic additives around Mg ions, and the role of reaction temperature  
226 (Table 1, Fig. 5). For all of these experiments, the pH decreased from 12.4 to 9 in the first 10  
227 minutes and then continued to decrease at a slower rate until stabilization to a value in the range  
228 5.5-6 after 1 h of reaction. This result indicates that the pH was mainly controlled by inorganic  
229 carbonate speciation and  $\text{CO}_2$  pressure (Figs. SI-4 and 5), and that organic additives had a little or  
230 undetected influence. This result is in agreement with time-lapse Raman measurements where a  
231 protonation process of carbonate ions was also detected, indicating a pH change in the interacting  
232 solution (Figs. 1, 2). Conversely, organic additive has significant effect on the texture (crystal size)  
233 and structural water content of the mineral produced, as identified in recovered suspensions by  
234 Raman ex-situ measurements (Fig. 5). Hydromagnesite was the main mineral phase precipitated at  
235  $60^\circ\text{C}$  for 24 h in the absence or presence of organic additive. However, both the mineral texture,  
12

236 measured by the Full Width Half Maximum (FWHM) of the largest Raman peak, and the structural  
237 water content, measured by the position of largest Raman peak, were slightly different with respect  
238 to the reference of the hydromagnesite precipitated in a solution free of additive. In addition, some  
239 traces of magnesite were detected after 24 h of reaction when ferric EDTA or citric acid tri-sodium  
240 salt were used. For the EDTA additive, slow hydromagnesite-to-magnesite transformation was  
241 detected and about 7 days were required to obtain high-purity magnesite at 60°C. Only  
242 nesquehonite was detected at 25°C in the presence of EDTA (Fig. 5). This result confirms that  
243 magnesite precipitation from the aqueous carbonation of magnesium hydroxide at room  
244 temperature was inhibited, or strongly retarded, by the precipitation of nesquehonite.

245

### 246 *3.3 Environmental implications*

247 Magnesite formation at room temperature (<30°C) from the aqueous carbonation of magnesium  
248 hydroxide remains a scientific challenge. This formation could make the magnesite precipitation  
249 an economical issue to store permanently the CO<sub>2</sub> with important environmental advantages:

250 (1) reduce CO<sub>2</sub> emissions from the industrial sector (e.g. steel and cement industry, coal-fired  
251 power),

252 (2) obtain magnesite-rich or high-purity magnesite materials with an aggregate value (e.g.  
253 fabrication of roadbed materials, bricks, granular fill, fire-retardant building material) at low or  
254 moderate temperature and reduced time (<24 h) and,

255 (3) use of mine solid wastes (e.g., mines in ultrabasic rocks) or widely available Mg-silicates as a  
256 magnesium source to capture CO<sub>2</sub>.

257 In practice, the residual alkaline-solution used during magnesite production could be recycled for  
258 future carbonation experiments or re-used in other chemical processes, but these options were not

259 assessed in the present study.

260 In this context, the production of magnesite material as an effective solution to reduce the industrial  
261 CO<sub>2</sub> emission may be a serious option at industrial scale as now proposed by Cambridge Carbon  
262 Capture (<http://www.cacaca.co.uk/#news>).

263

#### 264 **4. Conclusion**

265 In the present study, we demonstrated that high-purity magnesite can be produced from the  
266 carbonation of magnesium hydroxide at a rate of about 6 kg/m<sup>3</sup>h, and thus a mineralization rate of  
267 CO<sub>2</sub> into magnesite of about 3kg/m<sup>3</sup>h. Higher productions were estimated for hydromagnesite (120  
268 kg/m<sup>3</sup>h) and nesquehonite (40 kg/m<sup>3</sup>h), but these minerals are thermodynamically less stable at  
269 Earth surface conditions than magnesite.

270 Our time-resolved Raman measurements allowed a detailed description of reaction mechanism and  
271 kinetics of carbonation of magnesium hydroxide in batch reactor conditions. This experimental  
272 setup offers new possibilities for investigating mineral condensation from ionic solutions and  
273 slurries, and for investigating other chemical reactions at the solid-fluid interfaces.

274

275

276

277

278

279

280

281

282 **Acknowledgements**

283

284           The authors acknowledge funding from the French National Centre for Scientific Research  
285 (CNRS). We thank Nathaniel Findling for technical assistance.

286

287

288

289

290

291

292

293

294

295

296

297

298

299

300



301 **References**

302 [1] Peters et al. Towards real time verification of CO<sub>2</sub> emissions Nature Climate Change 7  
303 (2017) 848-850. <https://doi.org/10.1038/s41558-017-0013-9>

304 [2] Montes-Hernandez et al. Mineral sequestration of CO<sub>2</sub> by aqueous carbonation of coal  
305 combustion fly-ash, Journal of Hazardous Materials 161 (2009) 1347-1354.

306 [3] Mediavilla et al. The transition towards renewable energies: Physical limits and temporal  
307 conditions. Energy Policy 52 (2013) 297-311.

308 [4] P. Berg, A. Boland, Analysis of Ultimate Fossil Fuel Reserves and Associated CO<sub>2</sub>  
309 Emissions in IPCC Scenarios. Natural Resources Research 23 (2014) 141-158.

310 [5] G. Montes-Hernandez, F. Renard, R. Lafay, Experimental assessment of CO<sub>2</sub>-mineral-toxic  
311 ion interactions in a simplified freshwater aquifer: Implications for CO<sub>2</sub> leakage from deep  
312 geological storage. Environmental Science & Technology 47 (2013) 6247-6253.

313 [6] S. Bai, Q. Shao, P. Wang. Q. Dai, X Wang, X. Huang, Highly Active and Selective  
314 Hydrogenation of CO<sub>2</sub> to Ethanol by Ordered Pd–Cu Nanoparticles. J. Am. Chem. Soc. 139 (20)  
315 (2017) 6827-6830.

316 [7] M. B. Ross, C. T. Dinh, Y. Li, D. Kim, P. De Luna, E. H. Sargent, P. Yang, Tunable Cu  
317 Enrichment Enables Designer Syngas Electrosynthesis from CO<sub>2</sub>. J. Am. Chem. Soc. 139 (27)  
318 (2017) 9359-9363.

319 [8] G. Montes-Hernandez, F. Renard, R. Chiriac, N. Findling, F. Toche, Rapid precipitation of  
320 magnesite micro-crystals from Mg(OH)<sub>2</sub>-H<sub>2</sub>O-CO<sub>2</sub> slurry enhanced by NaOH and a heat-ageing  
16

321 step (from ~20 to 90°C). *Crystal Growth & Design* 12 (2012) 5233-5240.

322 [9] G. Montes-Hernandez, G. Sarret, R. Hellmann, N. Menguy, D. Testemale, L. Charlet, F.  
323 Renard, Nanostructured calcite precipitated under hydrothermal conditions in the presence of  
324 organic and inorganic selenium. *Chemical Geology* 290 (2011) 109-120.

325 [10] National Academies of Sciences, Engineering, and Medicine. 2019. *Gaseous Carbon*  
326 *Waste Streams Utilization: Status and Research Needs*. Washington, DC: The National Academies  
327 Press. <https://doi.org/10.17226/25232>.

328 [11] O. S. Pokrovski, S. V. Golubev, J. Schott, A. Castillo, Calcite, dolomite and magnesite  
329 dissolution kinetics in aqueous solutions at acid to circumneutral pH, 25 to 150 C and 1 to 55 atm  
330  $p\text{CO}_2$ : New constraints on  $\text{CO}_2$  sequestration in sedimentary basins. *Chem. Geol.* 265 (2009) 20-  
331 32.

332 [12] J. C. Deelman, Breaking Ostwald's rule. *Chemie Der Erde-Geochemistry* 61 (2001) 224-  
333 235.

334 [13] C. Pimentel, C. M. Pina, The formation of the dolomite-analogue norsethite: Reaction  
335 pathway and cation ordering. *Geochim. Cosmochim. Acta* 142 (2014) 217-223.

336 [14] M. Hänchen, V. Prigobbe, R. Baciocchi, M. Mazzotti, Precipitation in the Mg-carbonate  
337 system-effects of temperature and  $\text{CO}_2$  pressure. *Chem. Eng. Sci.* 63 (2008) 1012-1028.

338 [15] J. Xu, C. Yan, F. Zhang, H. Konishi, H.; Xu, H. Teng, Testing the cation-hydration  
339 effect on the crystallization of Ca-Mg- $\text{CO}_3$  systems. *Proc. Natl. Acad. Sci.* 2013 doi:  
340 10.1073/pnas.1307612110.

341 [16] I. M. Power, P. A. Kenward, G. M. Dipple, M. Raudsepp, Room temperature magnesite  
342 precipitation. *Cryst. Growth Des.* 17 (2017) 5652-5659.

343 [17] E. Nduagu, I. Romao, J. Fagerlund, R. Zevenhoven, Performance assessment of producing  
344  $Mg(OH)_2$  for  $CO_2$  mineral sequestration. *Applied Energy* 106 (2013) 116-126.

345 [18] S. Madeddu, M. Priestnall, E. Godoy, R. V. Kumar, S. Raymahasay, M. Evans, R. Wang,  
346 S. Manenye, H. Kinoshita, Extraction of  $Mg(OH)_2$  from Mg silicate minerals with NaOH assisted  
347 with  $H_2O$ : implications for  $CO_2$  capture from exhaust flue gas. *Faraday Discussions* 183 (2015)  
348 369-387.

349 [19] G. Montes-Hernandez, F. Renard, Time-resolved in situ Raman spectroscopy of the  
350 nucleation and growth of siderite, magnesite and calcite and their precursors. *Crystal Growth &*  
351 *Design* 16 (2016) 7218-7230.

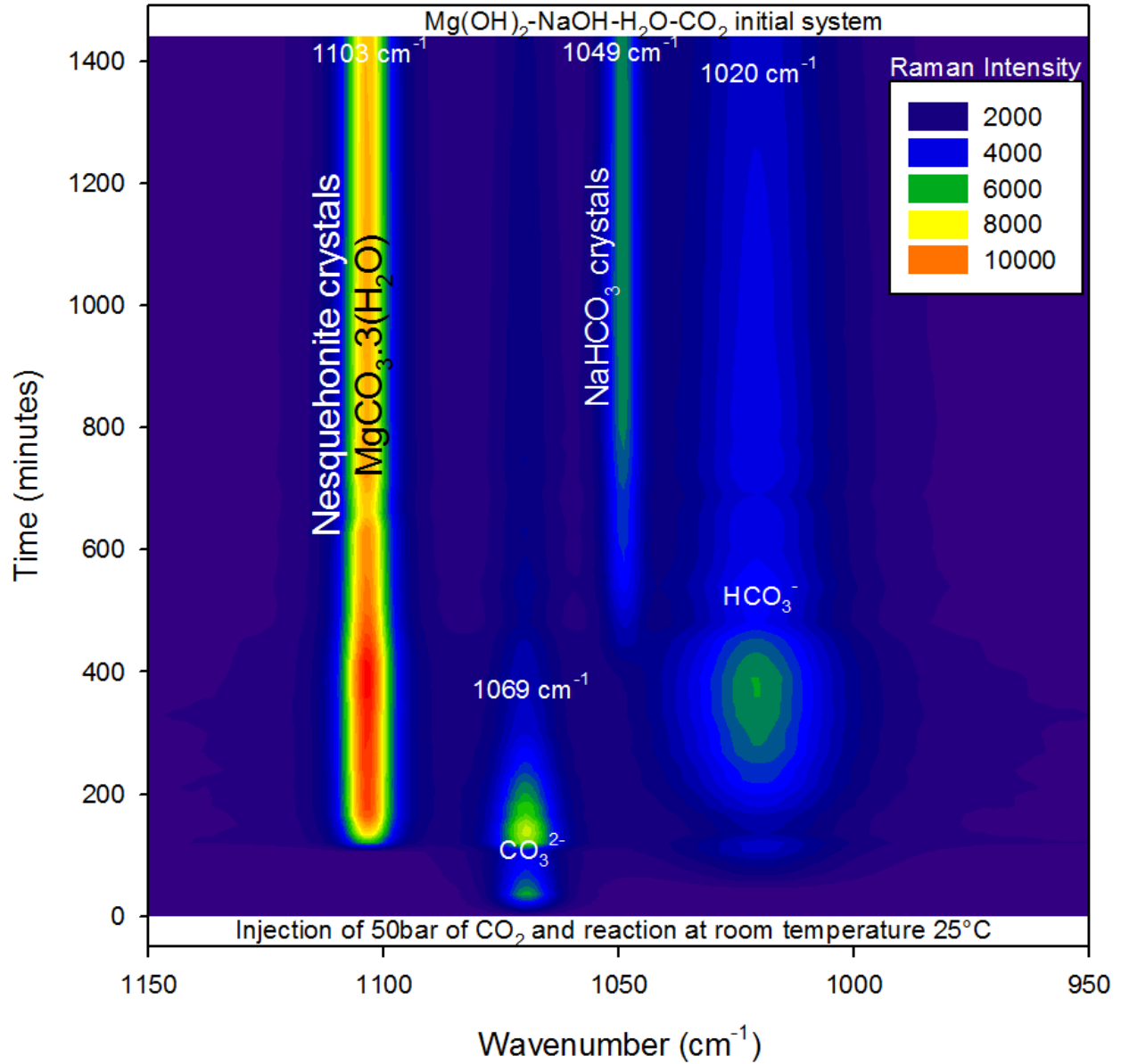
352

353

354 Table 1. Experiments of magnesium carbonates precipitation from Mg(OH)<sub>2</sub>-NaOH-H<sub>2</sub>O-CO<sub>2</sub>  
 355 slurry under anisobaric conditions (initial CO<sub>2</sub> pressure of 50bar).

Run	Temperature (°C)	Additive (1g)	Real-time monitoring	Exp. Duration (h)	Mineral transient phase(s)	Final mineral phase(s)
1	25	-	Raman spectroscopy	72	none	nesquehonite
2	90	-	Raman spectroscopy	24	hydromagnesite	magnesite
3	90	-	pH probe	24	N/A	Magnesite and residual hydromagnesite
4	60	-	pH probe	24	N/A	hydromagnesite
5	60	citric acid	pH probe	24	N/A	hydromagnesite
6	60	aspartame	pH probe	24	N/A	hydromagnesite
7	60	EDTA	pH probe	24	N/A	hydrogmagnesite
8	60	EDTA	pH probe	72	N/A	magnesite and hydromagnesite
9	60	EDTA	pH probe	168	N/A	magnesite
10	25	EDTA	pH probe	168	N/A	nesquehonite

356



357

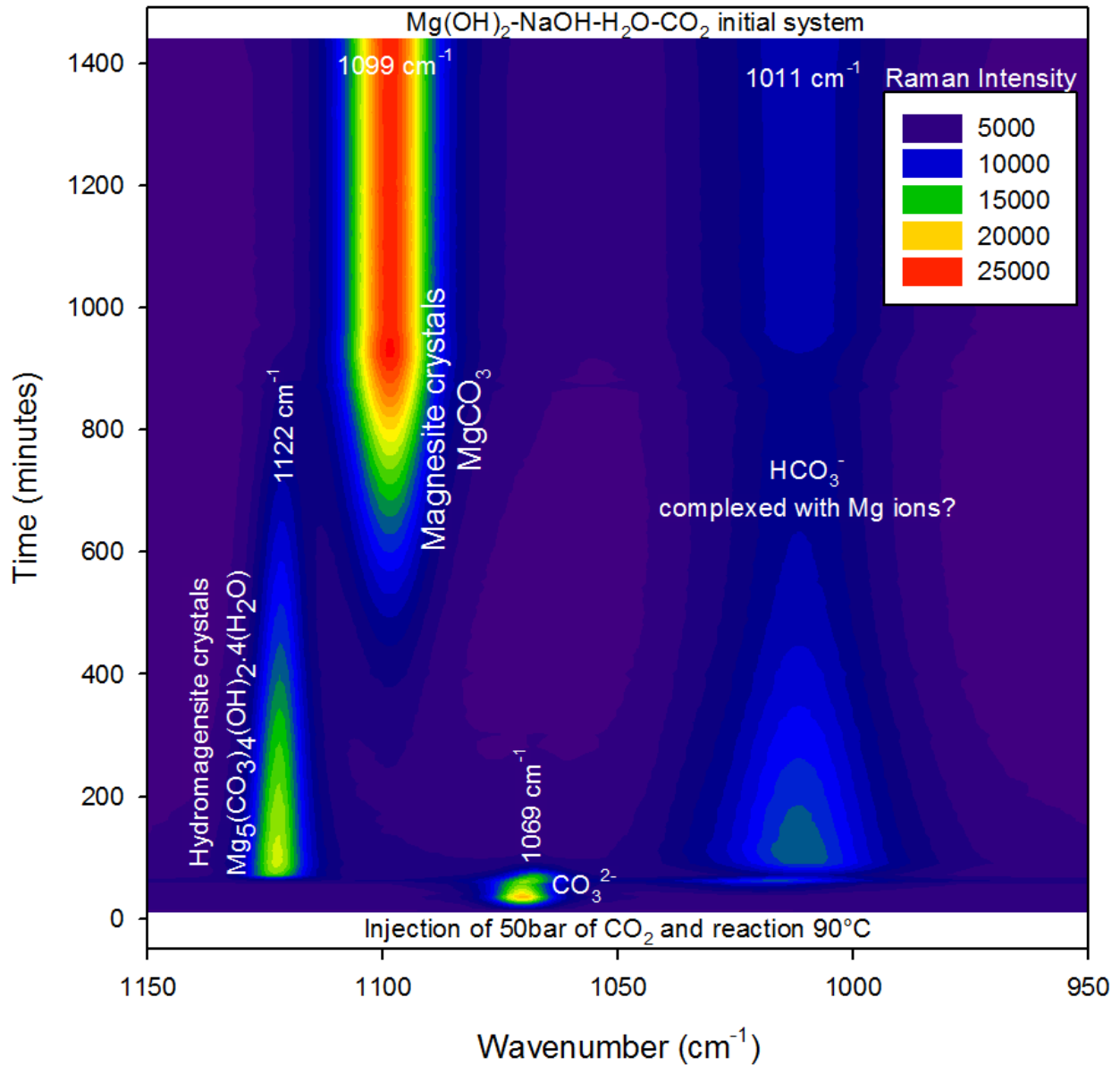
358 Figure 1. Time-lapse Raman spectroscopy monitoring of the aqueous carbonation of magnesium

359 hydroxide at 25 °C under anisobaric conditions. The positions of the Raman peaks and the

360 corresponding aqueous or mineral species are indicated on the figure.

361

362



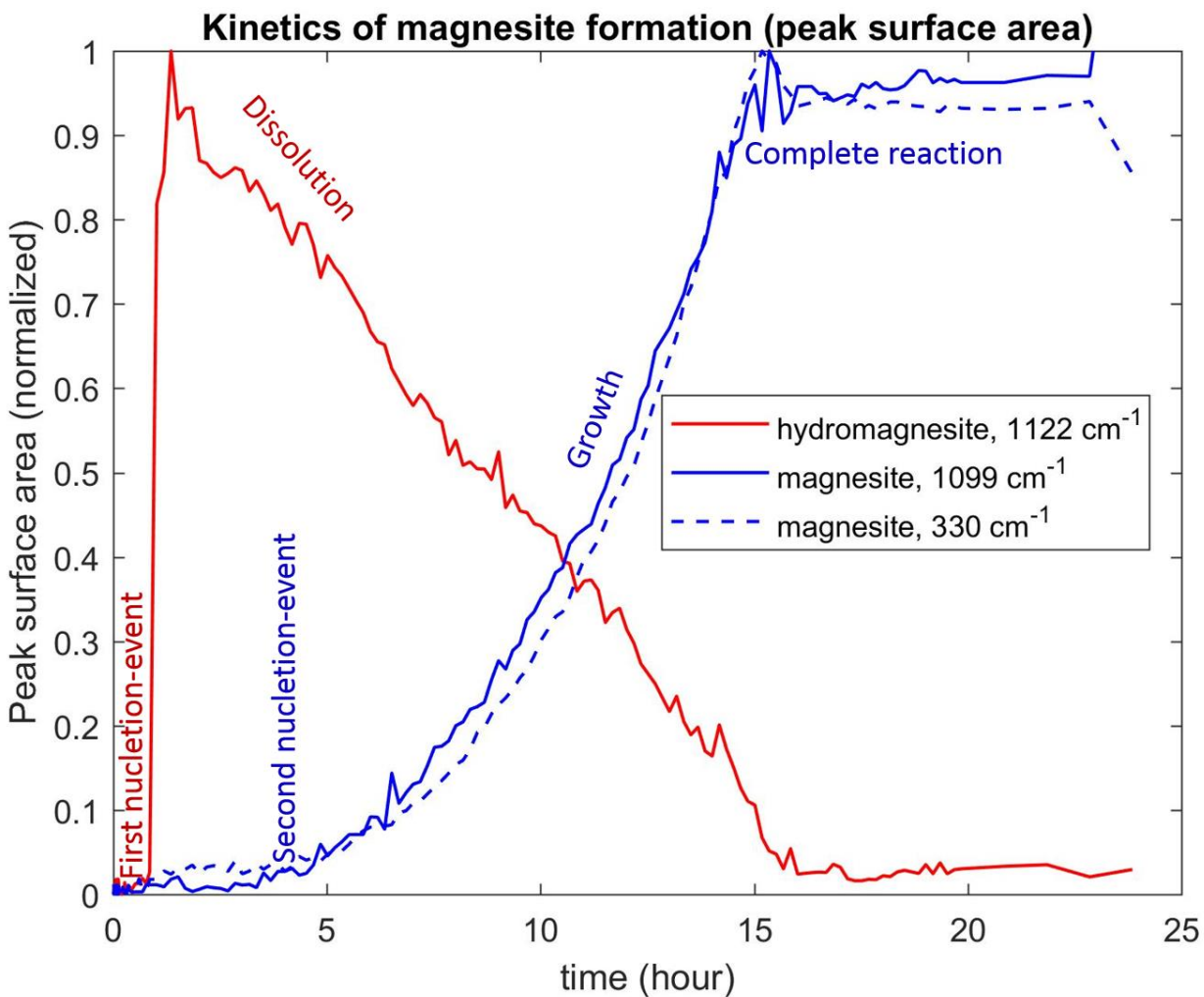
363

364 Figure 2. Time-lapse Raman spectroscopy monitoring of the aqueous carbonation of magnesium

365 hydroxide at 90°C under anisobaric conditions. The positions of the Raman peaks and the

366 corresponding aqueous or mineral species are indicated on the figure. The same data are shown on

367 Fig. SI-2 in the form of spectra.



369

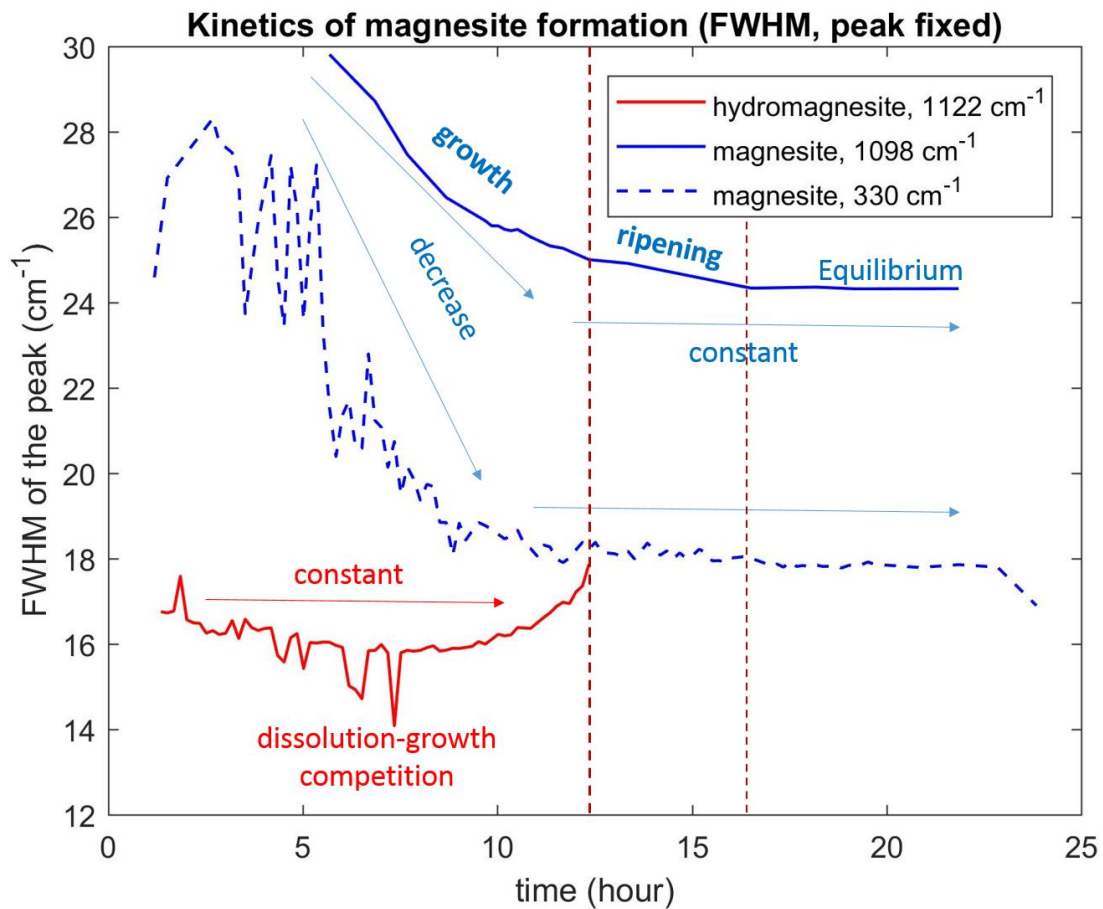
370 Figure 3. Kinetics of nucleation and growth of hydromagnesite and magnesite during aqueous

371 carbonation of magnesium hydroxide at 90°C measured by Raman spectroscopy. The peak surface

372 area is calculated as a function of time for one Raman peak of hydromagnesite and two Raman

373 peaks for magnesite, from the data shown in Figs. 2 and SI-2.

374

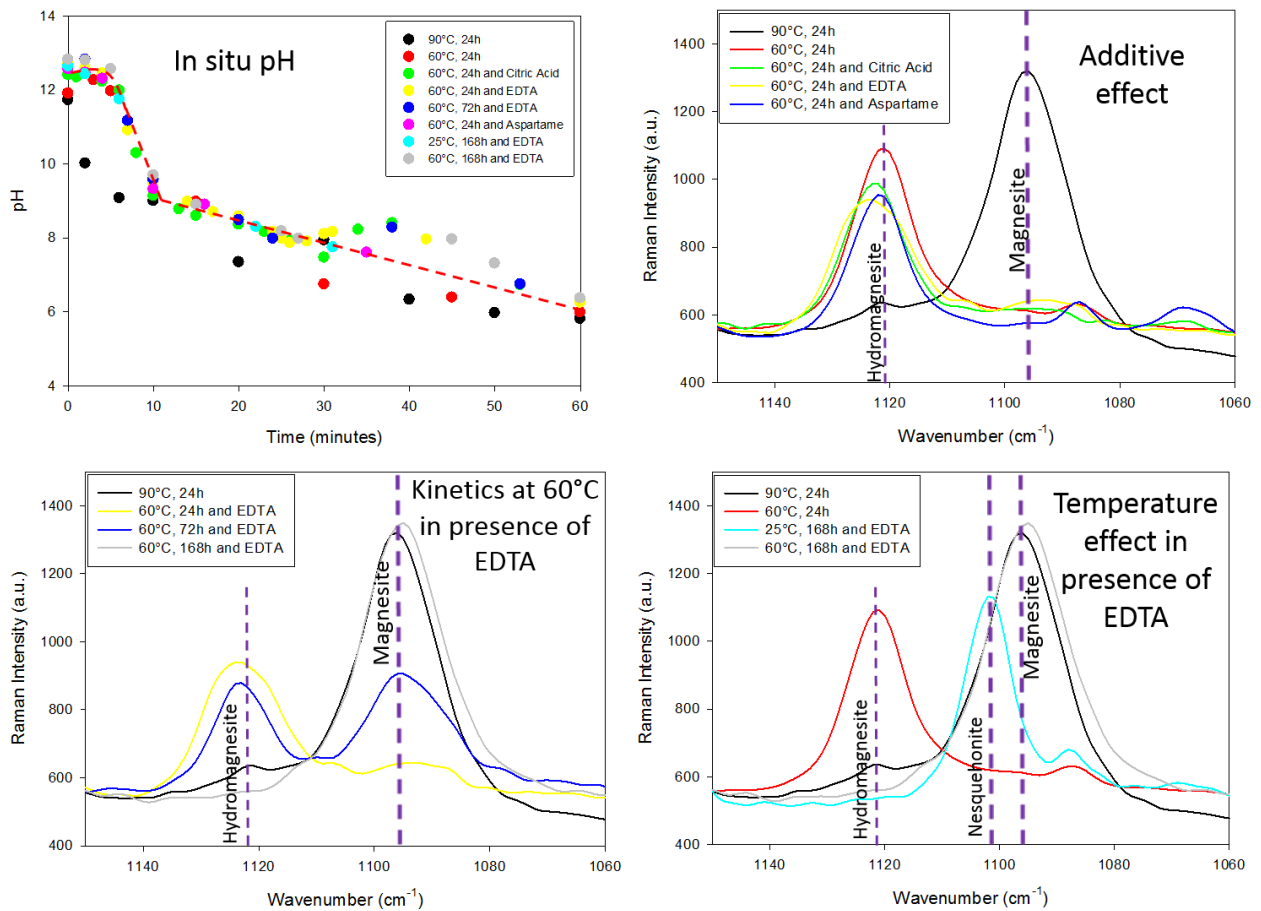


375

376 Figure 4. Crystal growth mechanism of magnesite (blue) at  $90^\circ\text{C}$ , nourished by hydromagnesite  
 377 dissolution (red) and measured by the Full Width at Half Maximum (FWHM) of the Raman peaks  
 378 shown in Figs. 2 and SI-2.

379





380  
 381 Figure 5. pH measured in-situ during aqueous carbonation of magnesium hydroxide in eight  
 382 experiments (Table 1), with or without additive. Influence of organic additives and temperature on  
 383 the aqueous carbonation of magnesium hydroxide (Mg(OH)<sub>2</sub>-NaOH-H<sub>2</sub>O-CO<sub>2</sub> slurry) under  
 384 anisobaric conditions.

385